Monsoon Asia Rice Calendar (MARC): a gridded rice calendar in monsoon Asia based on Sentinel-1 and Sentinel-2 images

Xin Zhao[1], Kazuya Nishina[1], Haruka Izumisawa[2], Yuji Masutomi[3], Seima Osako[4], Shuhei Yamamoto[4]

[1]Biogeochemical Cycle Modeling and Analysis Section, Earth System Division, National Institute for Environmental Studies, 16-2 Onogawa, Tsukuba, Ibaraki, 305-8506, Japan
[2]Faculty of Life and Environmental Sciences, University of Tsukuba, 1-1-1 Tennodai, Tsukuba, Ibaraki, 305-8572, Japan
[3]Asia-Pacific Climate Change Adaptation Research Section, Center for Climate Change Adaption, National Institute for Environmental Studies, 16-2 Onogawa, Tsukuba, Ibaraki, 305-8506, Japan
[4]DATAFLUCT, Inc., 1-19-9 Dogenzaka, Shibuya, Tokyo, 150-0043, Japan

Correspondence to: Xin Zhao (zhao.xin@nies.go.jp) and Kazuya Nishina (nishina.kazuya@nies.go.jp)

Abstract. An accurate and spatially explicit large-scale rice calendar can enhance understanding of agricultural practices and their ecological services, particularly in monsoon Asia. However, currently available global- or continental-scale rice calendars suffer from coarse resolution, poor recording, and outdated information, which do not provide detailed and consistent information on rice phenology. To address this limitation, this study mapped a new (2019 to 2020) gridded (0.5° × 0.5° resolution) rice calendar for monsoon Asia based on Sentinel-1 and Sentinel-2 satellite images. The novelty of this rice calendar lies in the development of a consistent optimal methodological framework that allows spatially explicit characterization of the rice transplanting date, harvest date, and number of rice croppings. The methodological framework incorporates two steps: (1) detection of rice phenological dates and number of rice croppings through combination of a feature-based algorithm and the fitted Weibull function, and (2) spatio-temporal integration of the detected transplanting and harvest dates derived from step 1 using von Mises maximum likelihood estimates. Results revealed that the proposed rice calendar can accurately identify the rice phenological dates for three croppings in monsoon Asia. When compared with single rice data from the census-based RiceAtlas ~~rice~~ calendar, the proposed ~~rice~~ calendar ~~outperformed~~ exhibited better results than the MODIS-based RICA ~~rice~~ calendar. It exhibited bias of 4 and −6 days for transplanting and harvest dates, respectively, with ~~marked improvement~~ lower values in MAE by 10 and 15 days, and in RMSE by 6 and 15 days for transplanting and harvest dates, respectively. In total, the proposed rice calendar can detect single, double, and triple rice cropping with area of 0.53, 0.45, and 0.09 million of km^2, respectively. This novel gridded rice calendar fills the gaps in half-degree rice calendars across major global rice production areas, facilitating research on rice phenology that is relevant to the climate change. The developed gridded Monsoon Asia Rice Calendar (MARC) ~~rice calendar for monsoon Asia~~ is available at https://www.nies.go.jp/doi/10.17595/20230728.001-e.html (Zhao and Nishina, 2023).

1 Introduction

A rice calendar records a series of phenological dates for rice growth and indicates the number of times that rice is grown in a year (Mishra et al., 2021; Zhao et al., 2023). Rice calendars provide critical information that contributes to agricultural management, crop production prediction, and estimation of greenhouse gas (GHG) emissions (Laborte et al., 2017; Portmann et al., 2010; Sacks et al., 2010). Specifically, concern regarding the negative impacts of rice cultivation is increasing because irrigated rice paddy field is an important source of anthropogenic GHG emissions, contributing 8% and 11% of global methane and nitrous oxide emissions, respectively (Saunois et al., 2020; Jiang et al., 2019). The inundated period from transplanting date to harvest date derived from a rice calendar largely determines the quantity of GHG emissions (Ito et al., 2021). To accurately estimate GHG emissions related to rice cultivation and to establish appropriate reduction measures, a detailed rice calendar that depicts rice phenology dynamics is urgently needed, especially for monsoon Asia, which accounts for 87% of the area of harvested rice globally and for 90% of global rice production (FAOSTAT, 2022).

Existing approaches to rice calendar mapping can be grouped into three categories: those based on census data, those based on models, and those based on remote sensing images. The limited number of global rice calendars (e.g., SAGE (Sacks et al., 2010), MIRCA2000 (Portmann et al., 2010), and RiceAtlas (Laborte et al., 2017)) that are currently available~~, which rely~~ relies on compilation of statistical data at national and/or sub-national scales. Model-based rice calendars (Waha et al., 2012; Elliott et al., 2015; Mathison et al., 2017; Iizumi et al., 2019) provide large-scale spatially explicit rice phenology information that is mainly based on climate data, but they are difficult to validate using earth observation data over such scales (Mishra et al., 2021). In contrast, remote sensing approaches that can provide consistent detection of large-scale rice phenological change over time have been used for rice calendar mapping with varying spatial coverage (e.g., global (Kotsuki and Tanaka, 2015), Asia (Mishra et al., 2021; Zhang et al., 2022), South and Southeast Asia (More et al., 2016), China (Luo et al., 2020), and Japan (Sakamoto et al., 2005)).

However, many challenges hinder the production of accurate rice calendar using remote sensing approach. First, use of a coarse–moderate-resolution satellite sensor (e.g., AVHRR with approximately 5 km resolution and MODIS with 500 m resolution) or any single sensor (optical or synthetic aperture radar (SAR)) diminishes the accuracy of rice calendar mapping. The RICA rice calendar, produced using MODIS images, faces issues with rice paddy field sizes smaller than the 500 m sensor resolution (Mishra et al., 2021). Second, the rule-based algorithm currently in use for rice phenological date extraction depends on turning points or key nodes of vegetation indexes and backscattering (Xin et al., 2020), which are affected by the smoothing method and the parameters adopted. Additionally, existing algorithms like ChinaCropPhen1km for China (Luo et al., 2020) and EVI-related methods for Japan (Sakamoto et al., 2005) are limited to specific administrative areas. Some alternative algorithms like PhenoRice (Mishra et al., 2021) and LAI-related approaches (Zhang et al., 2022) aim to map rice phenology at large areas but may ignore the fine heterogeneity within administrative units. Third, determination of the number of rice

croppings is frequently biased. For example, some recent studies focused only on main rice cropping (Zhang et al., 2022) or determined rice cropping during specific time windows (Mishra et al., 2021), thereby excluding rice grown in other periods. Additionally, rice sometimes grows across years because double or triple rice croppings, making it difficult to determine the actual number of rice croppings. Although methods have been proposed for extracting the number of croppings through growing season peak detection (Kotsuki and Tanaka, 2015; Yan et al., 2019), much effort is required to reduce the uncertainty of bias in the peak caused by ratoons and/or noisy data (Liu et al., 2020).

The combination of optical and SAR sensors, utilizing the high spatial (10 m) and temporal (6 days for Sentinel-1, 5 days for Sentinel-2) resolution of Copernicus Sentinel images, benefits crop phenology monitoring by offering precise and timely information on phenological variations. A feature-based algorithm, proposed for large-scale rice phenology detection (Zhao et al., 2023), excels in utilizing backscattering (VH) and vegetation indices (Enhanced Vegetation Index (EVI) and Normalized Difference Yellow Index (NDYI)) derived from Sentinel-1&-2 images to reflect features related to rice cultivation such as flooding, maximum leaf area, and most yellowness around transplanting, heading, and harvest date. Additionally, this algorithm has successfully tracked rice phenological dates of different cropping systems (single, double, and triple croppings) and at different spatial scales (sub-nation, 0.5° gridcell, and site scales) (Zhao et al., 2023). Meanwhile, a fitted six-parametric Weibull function has successfully been adopted to depict the growth development of phytoplankton (Rolinski et al., 2007) and vegetation (Maciel-Nájera et al., 2020; Muñoz-Salazar et al., 2022). Because variation of greenness is a reasonable indicator of crop intensity, the ability of a fitted Weibull function to fit the beginning, peak, and end of the greenness cycle allows it to capture the number of rice croppings. Different from most widely used peak greenness detection methods, which depend on thresholds, derivatives, or inflection points for detection (Xin et al., 2020; Yang et al., 2020), the fitted Weibull function omits the noisy peaks, which means it can track the shape of the vegetation index time series. Moreover, the fitted Weibull function has been packaged in the R software, making detection of the number of rice croppings automatic. Therefore, a feature-based algorithm combined with a fitted Weibull function is suitable for extracting rice phenological dates and the number of rice croppings.

The objective of this study was to develop a new gridded rice calendar that highlights the following features: (a) consistent detection using remote-sensing methods, (b) spatial resolution (0.5° × 0.5°), (c) large-scale coverage (monsoon Asia), and (d) ability to extract multiple rice croppings. To achieve this goal, Sentinel-1 and Sentinel-2 satellite images with high spatio-temporal resolution, spanning 2019 to 2020, were integrated within a novel methodological framework. This framework consists of two main steps: (1) detection of rice phenological dates and the number of rice croppings using a combination of a feature-based algorithm and a fitted Weibull function, and (2) spatio-temporal integration of detected phenological dates using von Mises maximum likelihood estimates. The resulting rice calendar was then evaluated against existing rice calendars. The findings of this study provide valuable insight into the methodological framework and rice calendar products, benefiting both crop calendar algorithm developers and end users.

2 Materials and methods

2.1 Study area

The analysed area is located in monsoon Asia, which ~~covered~~covers the region of 10° S to 53.5° N, 61° E to 153° E. The total area of monsoon Asia is 2106 millions of ha.

Monsoon Asia accounts for the largest rice harvested area and the greatest volume of rice production globally (Zhang et al., 2020). The rice paddy fields of monsoon Asia are mainly on the Indo-Gangetic Plain, the Yangtze Plain, the Ayeyarwady Delta region, and the Mekong Basin (Zhang et al., 2020). India and China have the two largest rice harvested areas covering 44 and 30 millions ha, respectively, followed by Bangladesh, Thailand, Vietnam, Myanmar, Philippines, Cambodia, Pakistan, and Nepal (Fig. S1) (FAOSTAT, 2022).

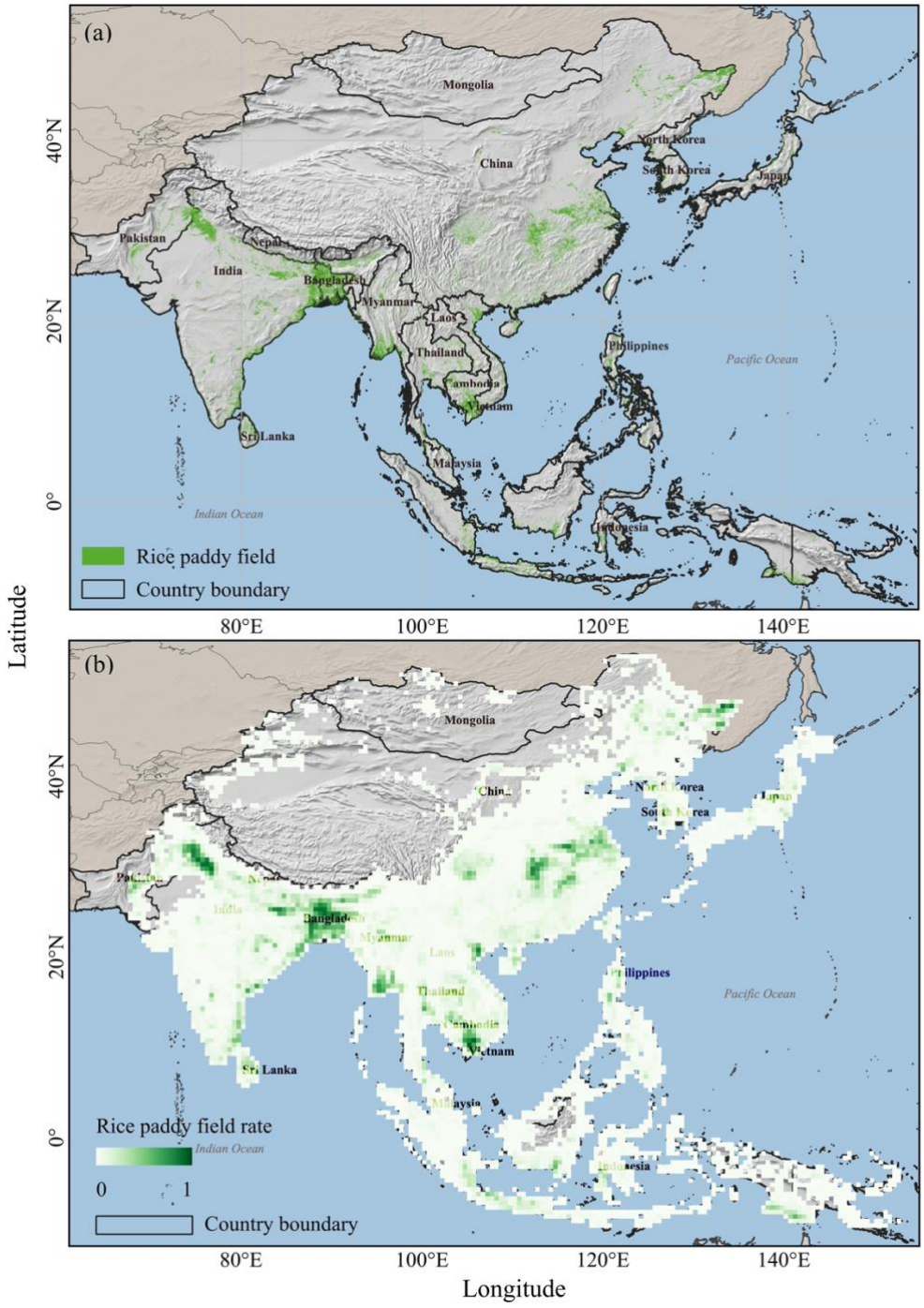

110

Figure 1. Location of the study area and distribution of rice paddy fields in monsoon Asia. Rice paddy field distribution map **(a)** was obtained from Zhang et al. (2020), which was produced using MODIS images. Green areas indicate rice paddy fields, and bold black borders indicate the countries in this study area. Gridded rice paddy field map **(b)** shows the percentage of rice paddy field in 0.5° grids. Green gradient indicates variation in the percentage coverage of rice paddy fields.

2.2 Data

2.2.1 Rice paddy field distribution map and sampling method

The rice paddy field distribution map adopted in this study is from a 500 m resolution map produced using MODIS images (Zhang et al., 2020) (Fig. 1a). This map effectively displays the presence and distribution of rice paddy fields over monsoon Asia. The reliability of this map is substantiated by its strong correlation with existing rice paddy field maps across diverse areas (R^2 values ranging from 0.72 to 0.95) and its alignment with the area information obtained from FAOSTAT statistical data for each country (Zhang et al., 2020). In this study, this rice paddy field distribution map was aggregated to a gridded map with 0.5° resolution (Fig. 1b).

Within each 0.5° grid, 20 rice paddy fields were randomly selected to derive the average rice phenology for that grid (Xiao et al., 2021; Zhao et al., 2023). This sampling method effectively minimizes errors caused by misclassification of rice paddy fields by excluding outliers that deviate from the averaged rice phenology (Zhao et al., 2023). Additionally, this sampling size of 20 rice paddy fields is sufficiently enough that saves computation time and has no effect on averaged rice phenology detection (Fig. S2).

2.2.2 Satellite data

All available images from Sentinel-1 and Sentinel-2 from 1 January 2019 to 31 December 2020 were used for generating backscattering or vegetation index time series via the Google Earth Engine (GEE) and the Google Colaboratory platforms. To overcome inherent speckle noise and overlapping observations of Sentinel-1 images, 3 × 3 pixels moving window filter and incidence angle processing were performed (Inoue et al., 2020). Invalid observations of Sentinel-2 images caused by clouds and cirrus were removed using cloud filtering (> 50%) and the cloud-score method (QA60 quality assessment band with 60 m resolution) (Inoue et al., 2020). The VH C-band Ground Range Detected images in the Interferometric Wide Swath mode were acquired with 6 day temporal resolution. Based on the Sentinel-2 Multispectral Instrument Level-1C top of atmosphere reflectance images, the EVI and the NDYI, based on the blue (B2), green (B3), red (B4), and NIR (B8) spectral bands with 10 m spatial resolution and 5 day temporal resolution, were calculated as follows:

$$EVI = \frac{2.5 \times (NIR - Red)}{NIR + 6 \times Red - 7.5 \times Blue + 1}, \quad (1)$$

$$NDYI = \frac{(Green - Blue)}{(Green + Blue)}, \quad (2)$$

The Locally Estimated Scatterplot Smoothing (LOESS) method was further adopted to smooth the time series data. The span value was assigned as 0.075 and 0.2 to depict VH and the EVI/NDYI time series pattern.

2.2.3 Reference rice calendars

There are three widely accepted rice calendars currently available. The RiceAtlas rice calendar, based on compilation of multiple census data sources, provides the start, peak, and end of the transplanting and harvest dates, and the number of rice croppings at national or sub-national scales globally (Laborte et al., 2017). The RICA rice calendar, generated using MODIS images, maps the rice transplanting date, harvest date, and number of rice croppings at administrative units in Asia (Mishra et al., 2021). The SAGE rice calendar records the gridded rice transplanting and harvest dates of 2000 at 5 min spatial resolution, but only records two rice croppings (Sacks et al., 2010). Therefore, the RiceAtlas, RICA, and SAGE rice calendars were used in this study to evaluate the number of rice croppings. The RiceAtlas rice calendar, with its detailed phenological date range, was used to assess the performance of the proposed rice calendar in determining transplanting date and harvest date, evaluating it based on the coefficient of determination (R^2), bias error (Bias), Mean Absolute Error (MAE), and Root Mean Square Error (RMSE) (Supplementary Text 1).

2.3 Methodology

The overall methodology for rice calendar mapping, which is summarized in Fig. 2, can be divided into two steps. The first step is extraction of transplanting and harvest dates and detection of the number of rice croppings, depicted in Fig. 2 Step 1. The transplanting and harvest dates obtained in the first step (Step 1) require temporal and spatial integration for the generation of the rice calendar (Fig. 2 Step 2).

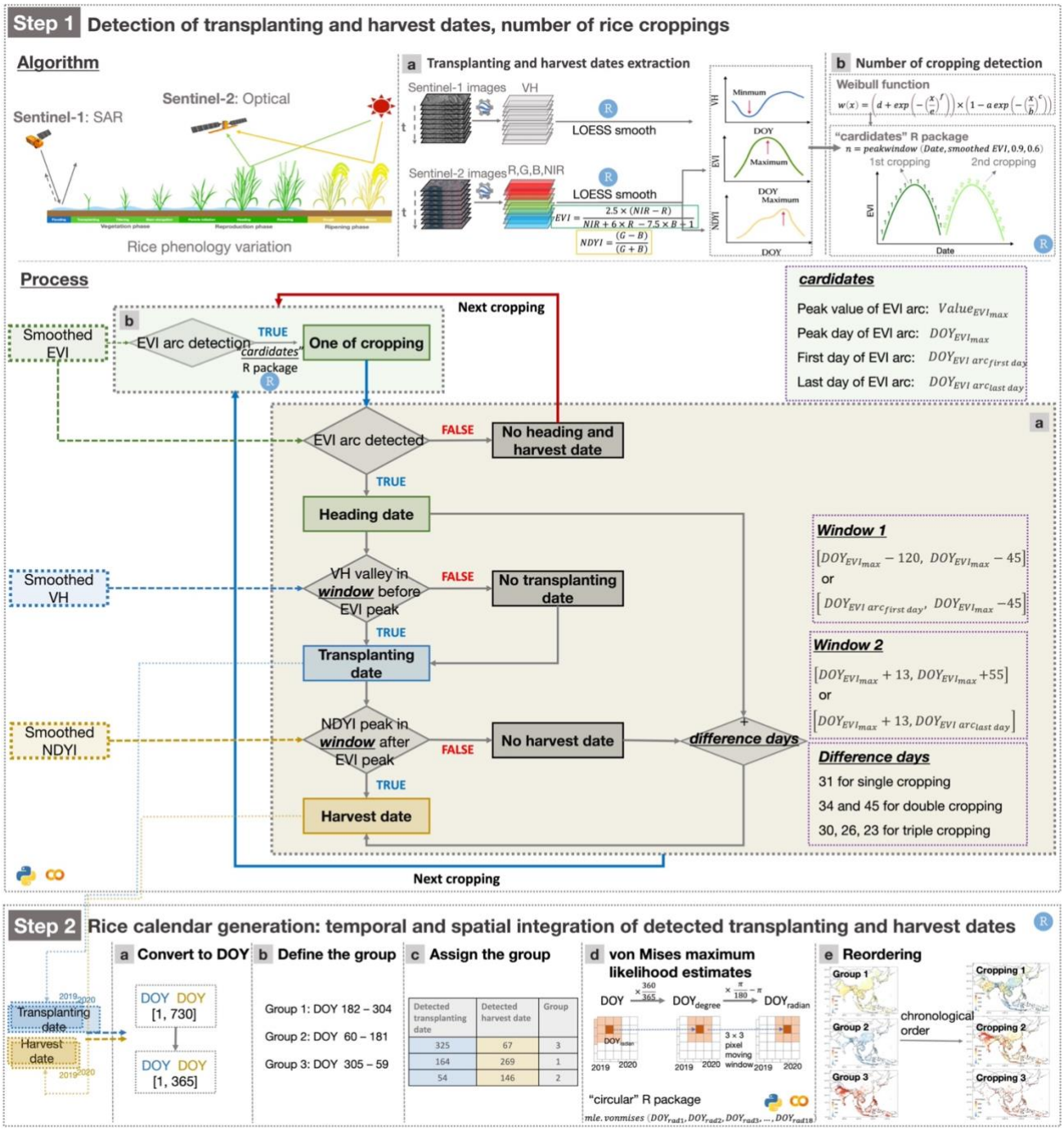

Figure 2. Workflow for gridded rice calendar mapping based on satellite images. Step 1 depicts the algorithm and process of transplanting and harvest dates extraction, along with the detection of number of rice croppings, as shown in the first box. In Step 2, the generation of the rice calendar is described, relying on the detected transplanting and harvest dates derived from Step 1, through the temporal and spatial integration of the detected phenological dates displayed in the second box.

2.3.1 Step 1: Extraction of phenological dates and number of rice croppings

2.3.1.1 Algorithm and process for extraction of transplanting and harvest dates

Flooding rice cultivation, common in Asia and accounting for over 12% of the global cropland (FAOSTAT, 2020; Zhang et al., 2021a), presents a distinctive flooding signal that can be used for detection of rice transplanting date. Additionally, rice harvest is characterized by irreversible leaf yellowing due to chlorophyll breakdown (Zhang et al., 2021b) (Fig. 2 Step 1 Algorithm). These phenological characteristics of rice crops can be captured by a feature-based algorithm applied on the smoothed VH, EVI, and NDYI time series data (Zhao et al., 2023). This algorithm's robustness has been confirmed at multiple spatial scales (sub-nation, 0.5° gridcell, and site scales) and cropping systems (single, double, and triple croppings) in monsoon Asia (Zhao et al., 2023). The transplanting date was determined by identifying the minimum VH intensity from the shortest plants above the water surface, where VH intensity gradually increase as they interact with the radar signal (Torres et al., 2012). The harvest date was detected using the NDYI's yellow signal, indicating the maximum yellowness at harvest date (Zhao et al., 2023) (Fig. 2 Step 1 Algorithm a).

The minimum VH and peak NDYI were detected within the time window (Fig. 2 Step 1 Process a), indicating that only the minimum VH and the maximum NDYI values within the time window, before and after the EVI peak, can be identified as the transplanting date and harvest date, respectively. To identify the optimal window for detection of the transplanting and harvest dates, the time window for detection of the minimum VH and peak NDYI were used (Table S1). ~~If the peak NDYI could not be obtained from those time windows, peak NDYI was identified using the peak EVI date ($DOY_{EVI_{max}}$) plus the corresponding difference days for each rice cropping, as referenced in Zhao et al. (2013) (Fig. 2 Step 1 Process a).~~ If the peak NDYI could not be obtained from those time windows, peak NDYI was identified using the peak EVI date ($DOY_{EVI_{max}}$) plus the difference days. The difference days for each rice cropping can be found in Zhao et al. (2023) (Fig. 2 Step 1 Process a).

2.3.1.2 Method and process for detecting the number of rice croppings

The six-parametric Weibull function can be used to identify the number of rice croppings by depicting an arc with the shape of downward-opening patterns from the smoothed EVI time series (hereafter referred to as EVI arc) (Fig. 2 Step 1 Algorithm b) as shown follows:

$$w(x) = \left(\mathrm{d} + \exp\left(-\left(\frac{x}{e}\right)^{f}\right)\right) \times \left(1 - a\exp\left(-\left(\frac{x}{b}\right)^{c}\right)\right) \quad (3)$$

where *a*, *b*, *c*, *d*, *e*, and *f* are the free parameters to be fitted (Rolinski et al., 2007).

This fitted Weibull function can be implemented using the peakwindow function in the "cardidates" package of R (Rolinski et al., 2007) (Fig. S3a; Fig. 3). The rice cropping duration and its peak were determined as follows:

$$Cropping = peakwindow\ (x, y, mincut, minpeak) \quad (4)$$

where y represents the variations of smoothed EVI time series values with respect to the date variable x.

To control the shape of the EVI arc, which represents the relative height between the neighbouring peaks and valleys, for the purpose of identifying rice cropping, the parameters *mincut* and *minpeak* were set to 0.9 (Figs. S3c and S4) and 0.6 (Figs. S3d and S4), respectively.

After application of the function (Eq. (4)), all available arcs of the smoothed EVI time series were ~~then~~ labelled, including the start (start day of detected EVI arc, $DOY_{EVI\ arc_{first\ day}}$), peak (peak day of detected EVI arc, $DOY_{EVI_{max}}$), and end (end day of detected EVI arc, $DOY_{EVI\ arc_{last\ day}}$) of the arc, and the peak EVI value ($Value_{EVI_{max}}$) (Fig. 2 Step 1 Process b).

This method can detect the EVI arc, even if it does not exhibit a complete downward-opening shape (Fig. S3b). This is because rice growth spans two years, and some days are not within the period of study, resulting in lack of EVI time series data for those days. Based on the labelled EVI arc, all rice croppings were recognized, as the heading date through extraction of the $DOY_{EVI_{max}}$.

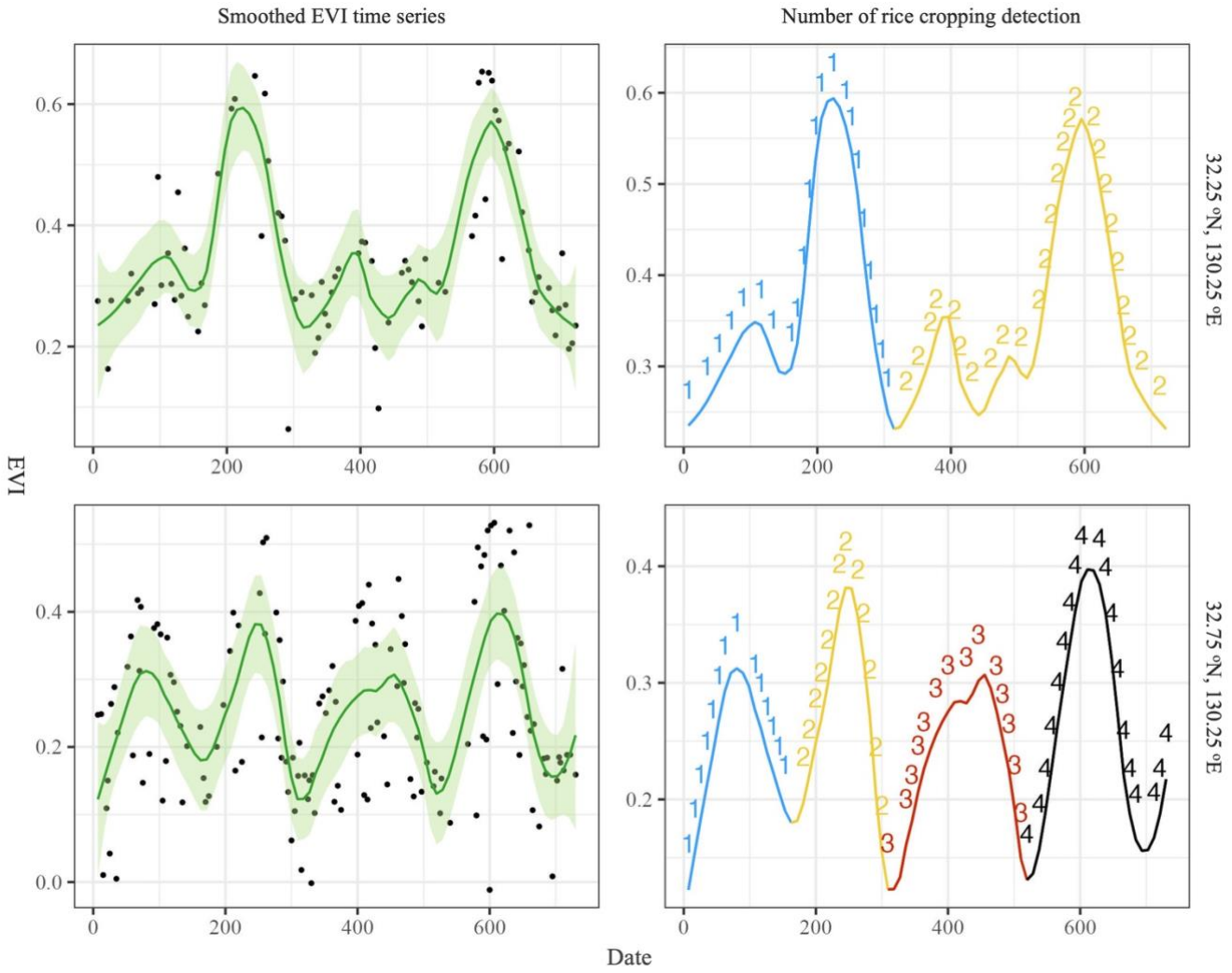

Figure 3. Smoothed EVI time series and subsequent identification of the number of rice croppings at adjacent grids (32.25°N, 130.25°E, and 32.75°N, 130.25E°) across two years. Left column shows the smoothed EVI time series using the LOESS method. Black points and green lines indicate the EVI value at specific dates and the smoothed EVI time series, respectively. Green area indicates the 95% confidence interval around the smoothed EVI time series. Right column displays the number of rice croppings detected using the fitted Weibull function implemented via the "cardidates" package in R. Blue, yellow, red, and black lines correspond to the detected first, second, third, and fourth arcs of the smoothed EVI time series.

2.3.2 Step 2: Temporal and spatial integration of detected transplanting and harvest dates for rice calendar generation

All the transplanting and harvest dates across two years for each grid were detected in Step 1 by using the algorithms and processes described above. However, these detected transplanting and harvest dates in each grid vary annually due to different weather conditions, the effects of climate change, adjustments in agricultural schedule, and the availability of satellite images. Additionally, the detected transplanting and harvest dates for a specific cropping season in a grid can differ markedly from

those in neighboring grids, possibly indicating detection errors. Therefore, the temporal and spatial integration of the detected transplanting and harvest dates, referred to as Step 2, is a necessary step for generation of a multi-year, spatially averaged rice calendar.

To achieve this goal, the first step involved converting all the detected transplanting and harvest dates over two years into the Day Of the Year (DOY) format, ranging from DOY 1 (1 January 2019) to DOY 730 (31 December 2020; 29 February 2020 was not considered for simplicity). Subsequently, the detected transplanting and harvest dates that occurred in 2020 (DOY 366 to DOY 730) were converted for consistency with the first year (DOY 1 to DOY 365) by subtracting 365 (Fig. 2 Step 2a). Finally, all the detected transplanting and harvest dates were converted to DOY values from 1 to 365 (Fig. 2 Step 2a).

The temporal and spatial integration of phenological dates should be conducted within specific periods of time. Typically, rice is cultivated up to three times annually in most areas (Mishra et al., 2021), which serves as a meaningful basis for dividing the year into three equal periods. Thus, the year was divided into three groups: Group 1: July–October (DOY 182 to DOY 304), Group 2: March–June (DOY 60 to DOY 181), and Group 3: November–February (DOY 305 to DOY 59) (Fig. 2 Step 2b). The detected phenological dates were assigned to the corresponding group based on the maximum number of days from the transplanting date to the harvest date falling within that group (Fig. 2 Step 2c).

The phenological date DOY values represent circular data that exhibit periodicity or cyclicity (Mahan, 1991). The designation of high and low values is arbitrary (Berens, 2009). For example, DOY 365 is almost the same as DOY 1 with 1 day difference instead of a difference of 364 days. Adoption of statistical analysis commonly used with circular data can lead to incorrect results, whereas the von Mises distribution $VM(\mu, \kappa)$ can display a circular unimodal distribution (Berens, 2009). The probability density function of the von Mises distribution can be expressed as follows:

$$p\ (x;\ \mu;\ \kappa) = \frac{1}{2\pi I_0(\kappa)}\, exp\ (\kappa \cos\ (x - \ \mu)) \quad (5)$$

where I_0 is the modified Bessel function of zero order, and for $-\pi \ll x \leq \pi$, $\kappa > 0$.

The availability of the "circular" R package (Agostinelli and Lund, 2023) is convenient for analysis of circular data. In the "circular" R package, the probability density function of the von Mises distribution can be displayed as follows:

$$qvonmises\ (x,\ mu,\ kappa) \quad (6)$$

where mu is the mean direction of the distribution, and $kappa$ is a non-negative numeric value representing a concentration parameter of the distribution; mu and $kappa$ are correspond to μ and κ in Eq. (5), respectively.

The circular data x in Eqs. (5) and (6) denote the phenological date shown in DOY format. The DOY was converted to an angle value (degrees) (Fig. 2 Step 2d) (Franch et al., 2022) as follows:

$$DOY_{deg} = \frac{DOY}{365} \times 360 \quad (7)$$

where DOY_{deg} represents the angular value of the DOY, and 365 denotes the number of equal interval date units representing one rotation around the circle.

The angle value of the DOY (DOY_{deg}) was then converted to the radian value of the DOY (DOY_{rad}) with interval $[-\pi, \pi]$ (Fig. 2 Step 2d) as follows:

$$DOY_{rad} = DOY_{deg} \times \frac{\pi}{180} - \pi = \frac{(DOY - 182.5) \times \pi}{182.5} \quad (8)$$

Then, DOY_{rad} was input into the mle.vonmises function in the "circular" R package to obtain the parameters of the von Mises distribution via maximum likelihood estimates. For each group (i.e., Group 1, Group 2, and Group 3), the DOY_{rad} of each grid and the eight neighbouring grids (3 × 3 pixel window) across the two years were included as input for the mle.vonmises function (Fig. 2 Step 2d). Overall, 18 DOY_{rad} values were used as follows:

$$res = mle.vonmises\ (DOY_{rad1}, DOY_{rad2}, DOY_{rad3}, \dots, DOY_{rad18}) \quad (9)$$

The parameters $DOY_{integrated}$ and Var were derived from the mle.vonmises function (Eq. (9)), representing the value and variance of the phenological dates (DOY_{rad}), respectively, after performing temporal and spatial integration for each grid within each group:

$$DOY_{integrated} = res\$mu \quad (10)$$

$$Var = res\$kappa \quad (11)$$

However, this value and variance of the phenological date ($DOY_{integrated}$ and Var) is a radian value, which must be converted back to the DOY (DOY_{mu} and DOY_{var}) as follows:

$$DOY_{mu} = DOY_{integrated} \times \frac{182.5}{\pi} + 182.5 \quad (12)$$

$$DOY_{var} = \frac{1}{Var} \times \frac{180}{\pi} / \frac{360}{365} = \frac{1}{Var} \times \frac{182.5}{\pi} \quad (13)$$

The integrated transplanting dates from all the groups (e.g., DOY_{mu_G1}, DOY_{mu_G2}, and DOY_{mu_G3}) were then reordered according to their chronological order for each grid. Finally, cropping-based phenological dates were obtained through the conversion of the group-based phenological dates (Fig. 2 Step 2e).

3 Results and discussion

3.1 Transplanting date and harvest date

Based on the above methodological framework, rice calendars with two types of transplanting and harvest dates were obtained: a group-based calendar (Fig. 4) and a cropping-based calendar (Fig. 6). The group-based rice calendar was initially produced, displaying explicit transplanting and harvest dates for three groups (Fig. 4). The median transplanting dates across monsoon Asia for the three rice groups are DOY 182, 77, and 325, with standard deviations of 23, 24, and 60, respectively (Fig. 4). Similarly, the median harvest dates for the three groups are 281, 172, and 67, with standard deviations of 23, 27, and 56, respectively (Fig. 4). Because the three groups divide the year equally, the transplanting date and the harvest date both exhibit a mono-peaked distribution (Fig. S5). Moreover, the variance of the transplanting or harvest dates observed in each grid originates from analysis of 18 detected transplanting or harvest dates from its eight neighbors across the two years, thereby highlighting both its temporal and spatial variations. The variance in transplanting and harvest dates across monsoon Asia for the three groups is shown in Fig. 5. The variance is 8, 11, and 12 for the transplanting dates and 7, 11, and 15 for the harvest dates (Fig. 5). These variances arise from interannual variation and spatial smoothing effect, and their small values indicate stability in phenological date extraction.

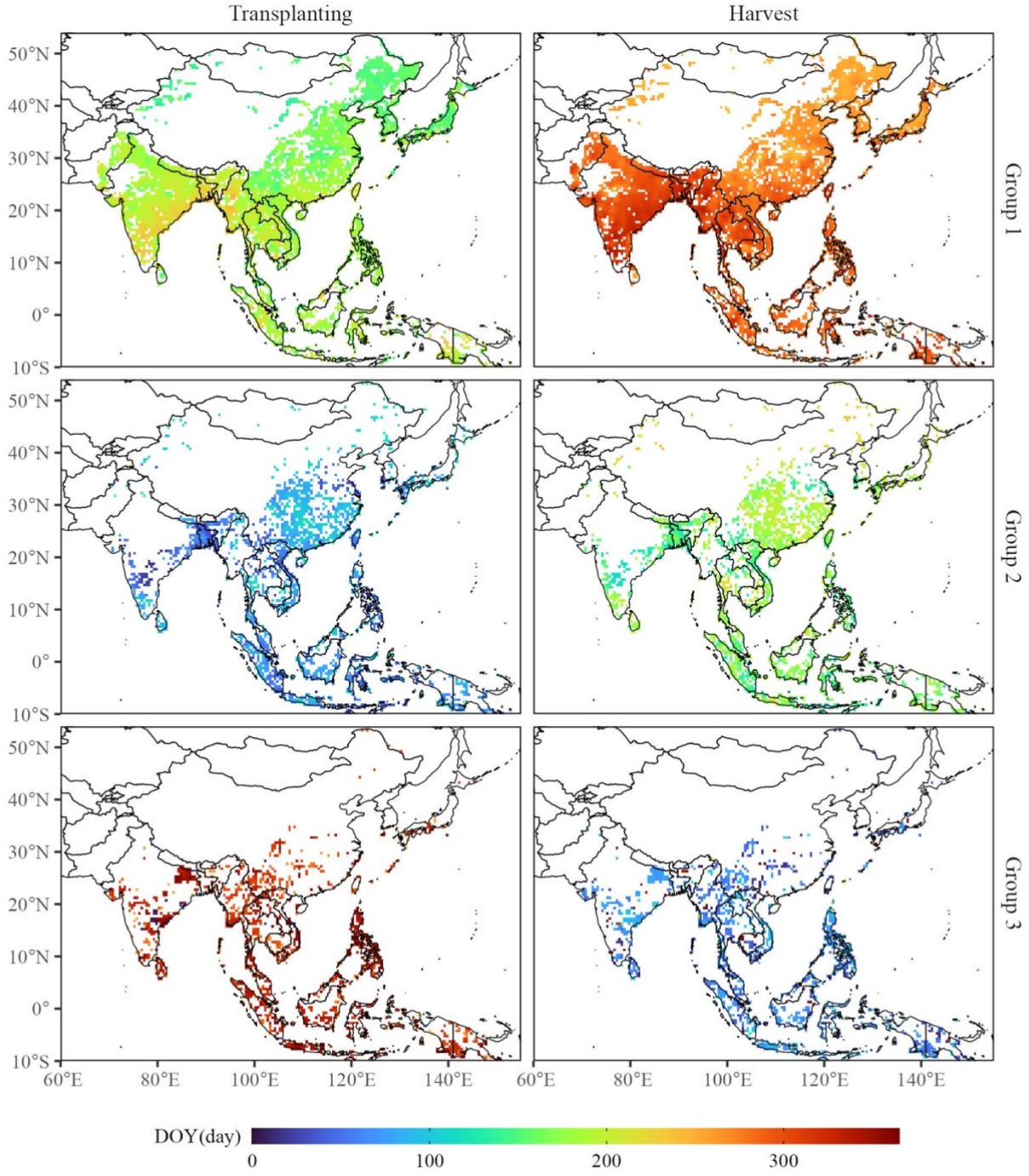

Figure 4. Transplanting date and harvest date for the three groups. Colour gradient from blue to red in the legend denotes the respective transplanting and harvest dates.

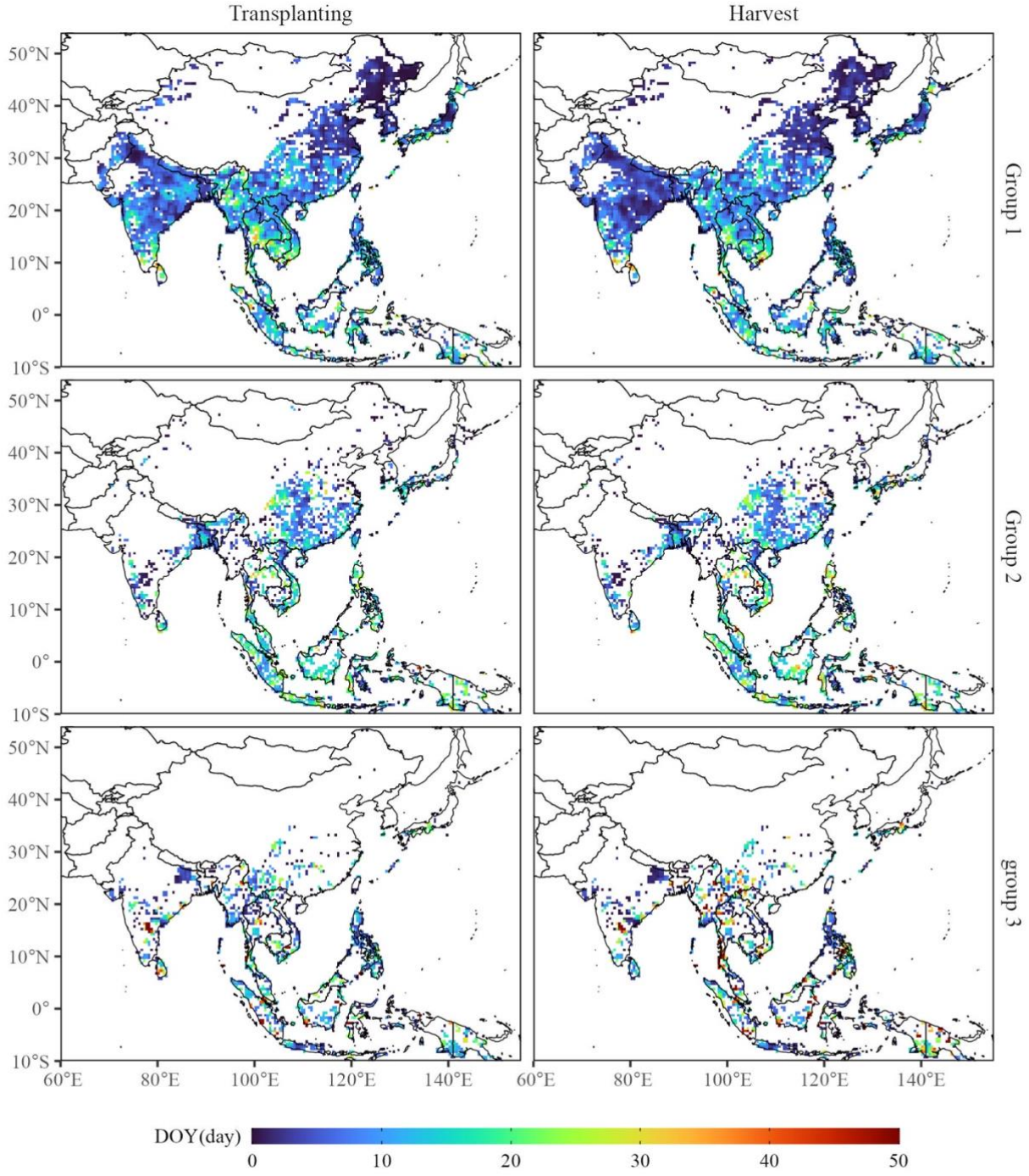

Figure 5. Variance in transplanting date and harvest date for the three groups. Colour gradient from blue to red in the legend denotes the respective variance in transplanting and harvest dates.

Then, the group-based transplanting and harvest dates were converted to the cropping-based format by reordering the detected transplanting dates for each grid. The cropping-based transplanting and harvest dates are in a common format that facilitates comparison with those of other rice calendars. The median transplanting dates across monsoon Asia for three rice croppings are DOY 154, 208, and 327, with standard deviations of 61, 68, and 27, respectively (Fig. 6). Similarly, the median harvest dates for three croppings are 253, 273, and 62, with standard deviations of 63, 111, and 47, respectively (Fig. 6). Owing to the large spatial coverage, the transplanting and harvest dates vary across different croppings, exhibiting a dual-peaked distribution (Fig. 8). The variance in transplanting dates for three croppings across monsoon Asia is 9, 10, and 12, while the variance in harvest dates is 8, 11, and 16 (Fig. 7).

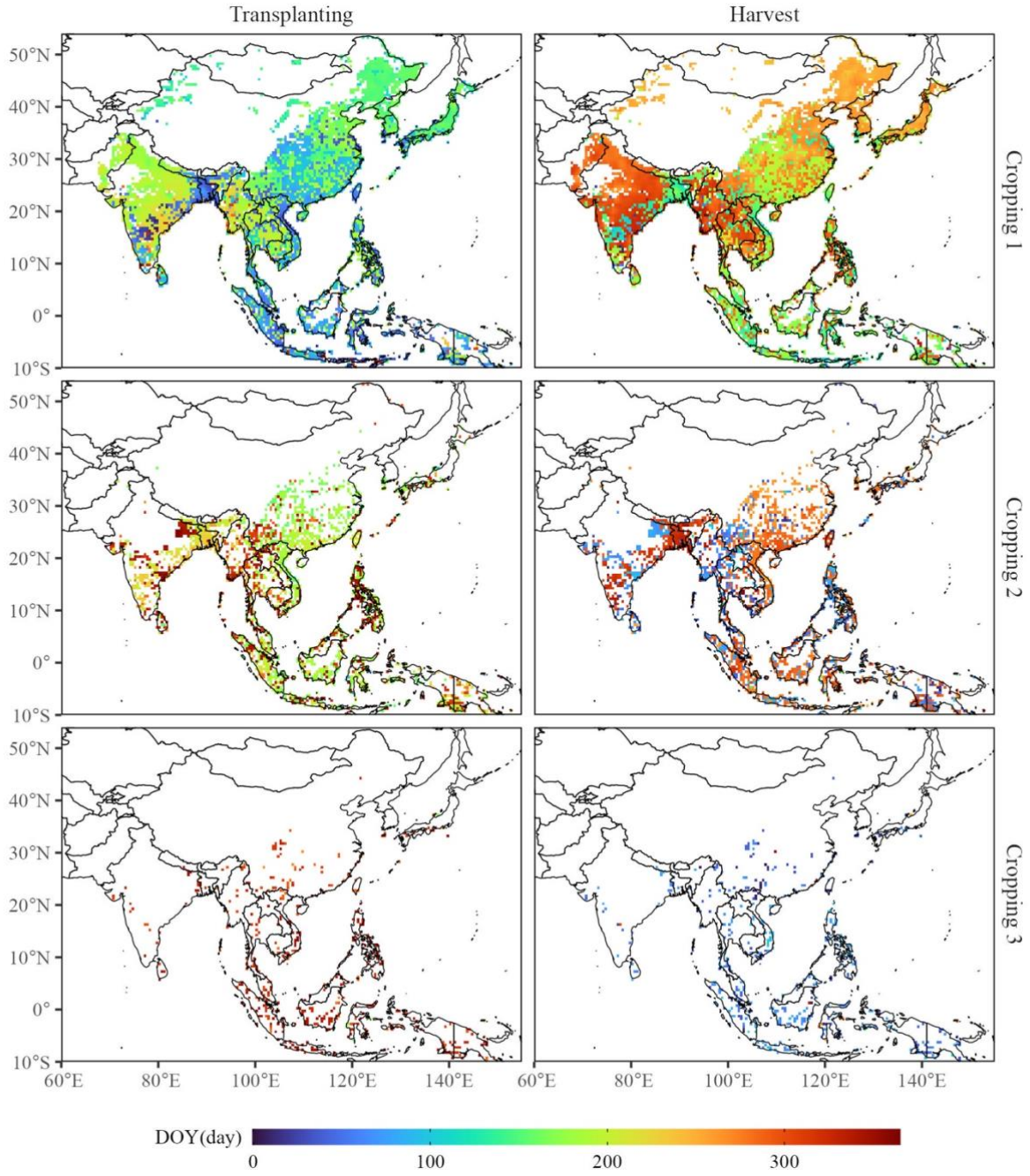

Figure 6. Transplanting date and harvest date for three rice croppings. Colour gradient from blue to red in the legend denotes the respective transplanting and harvest dates.

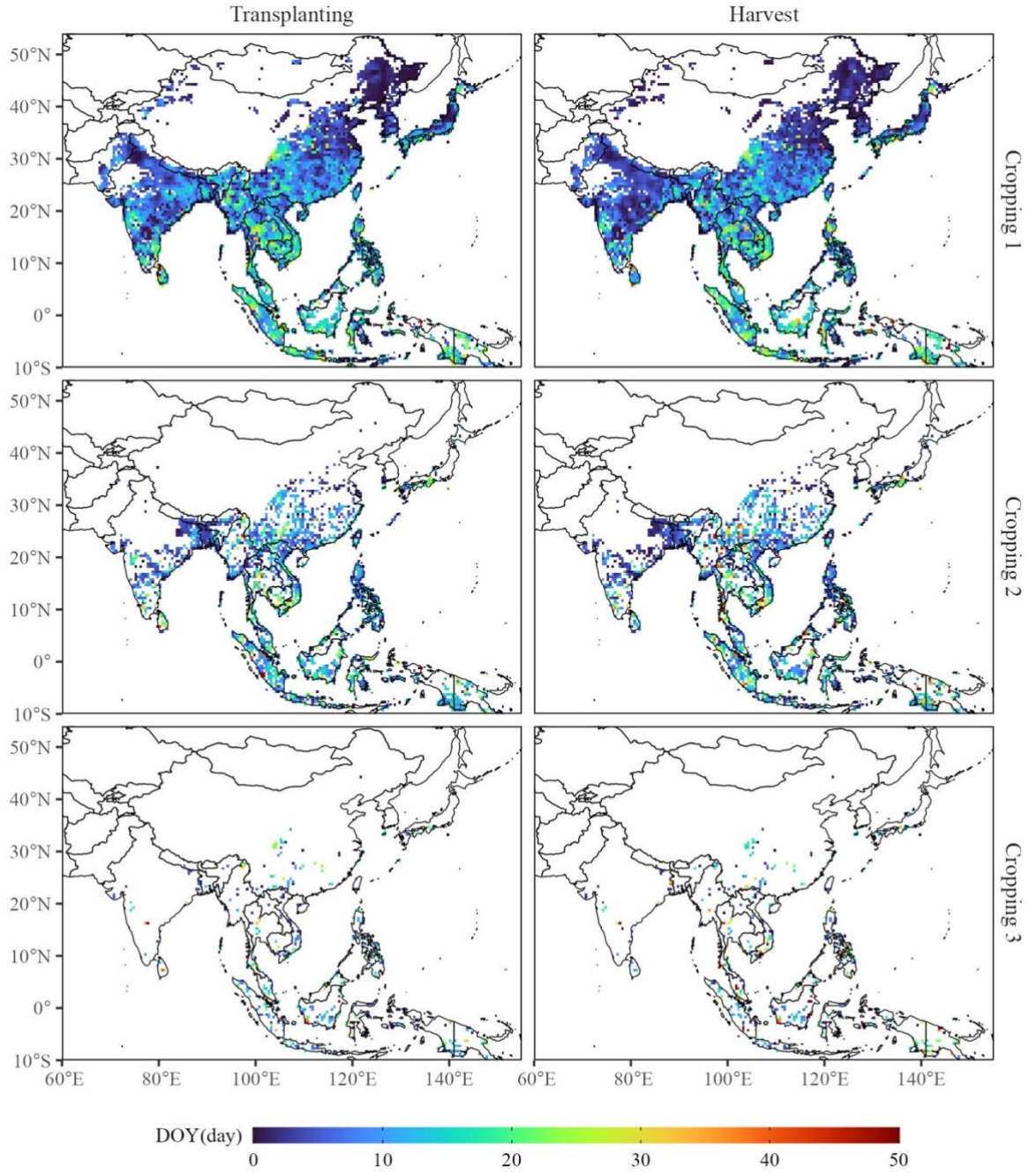

Figure 7. Variance in transplanting date and harvest date for three rice croppings. Colour gradient from blue to red in the legend denotes the respective variance in transplanting and harvest dates.

315

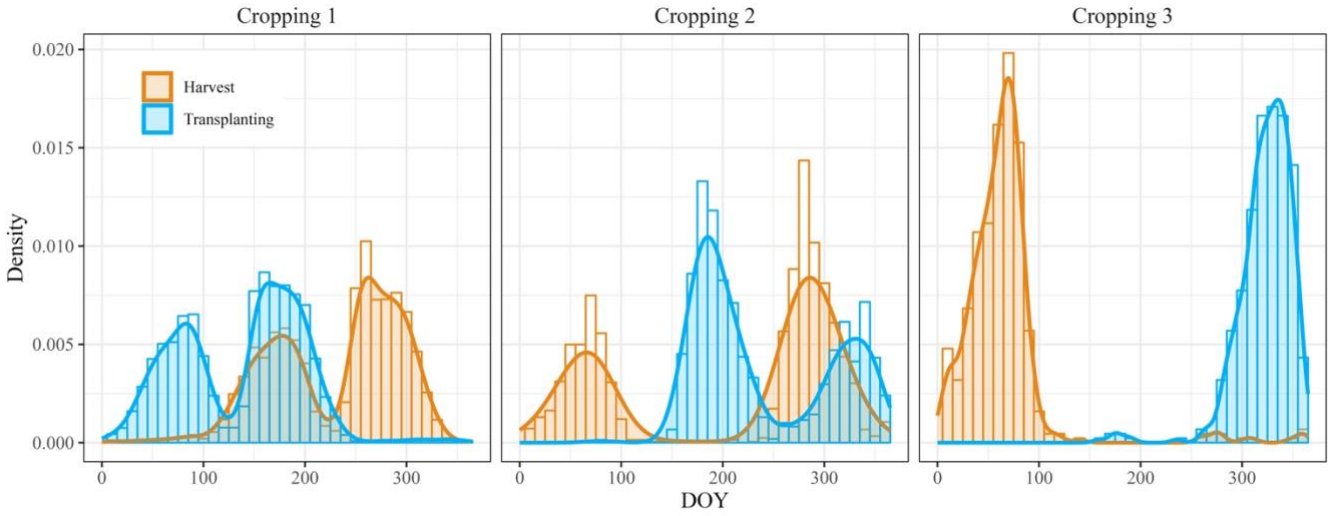

Figure 8. Distribution of transplanting and harvest dates for three rice croppings. Blue and orange represent the transplanting date and the harvest date, respectively.

There are difficulties in directly comparing transplanting and harvest dates with those from other rice calendars owing to differences in spatial resolution (grid versus administrative) and the identification of rice cropping sequences (Clauss et al., 2018). Thus, the RiceAtlas rice calendar, which has been rasterized to the same spatial resolution as that of the proposed rice calendar (0.5°), was used to evaluate the performance in terms of single rice cropping for the transplanting and harvest dates. The transplanting dates of the proposed rice calendar are consistent with those of the RiceAtlas rice calendar, with R^2 of 0.43, Bias of 3.93 days, MAE of 16.38 days, and RMSE of 27.62 days (Fig. 9). Additionally, the harvest dates of the proposed rice calendar are correlated with those of the RiceAtlas rice calendar, with R^2 of 0.44, Bias of −5.76 days, MAE of 17.87 days, and RMSE of 28.32 days (Fig. 9). However, the presence of the same transplanting or harvest dates across large spatial areas in the RiceAtlas rice calendar (Fig. S6) reduces its accuracy. Similarly, the RiceAtlas rice calendar has been used to evaluate the performance of the MODIS-based RICA rice calendar (Mishra et al., 2021). Compared to the RICA rice calendar in terms of accuracy, ~~The~~ the proposed rice calendar ~~outperforms~~ demonstrates a ~~the RICA rice calendar in terms of accuracy, with~~ smaller MAE (26.41 days in the RICA rice calendar) and RMSE (34.20 days in the RICA rice calendar) ~~in relation to~~ for transplanting dates, and almost half the MAE (33.20 days in the RICA rice calendar) and smaller RMSE (42.72 days in the RICA rice calendar) ~~in relation to~~ for harvest dates (Mishra et al., 2021).

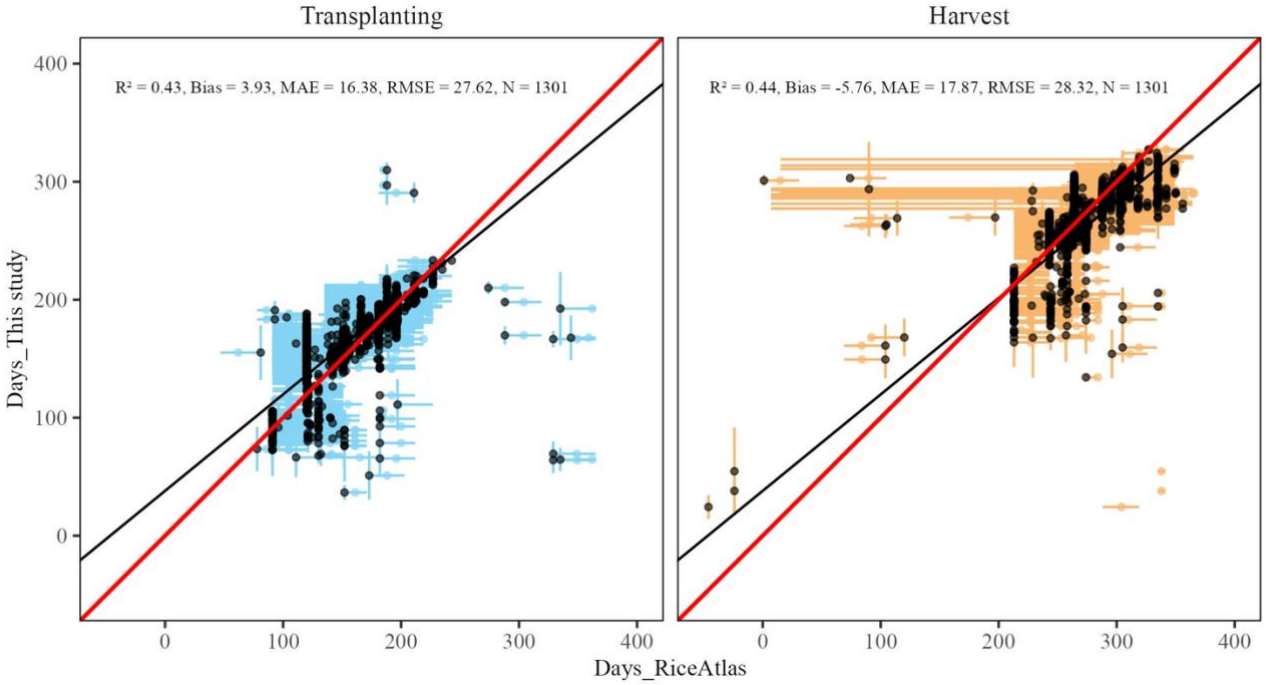

Figure 9. Comparison of transplanting date and harvest date for single rice cropping between the proposed rice calendar and the RiceAtlas rice calendar. Blue and orange represent the transplanting date and harvest date, respectively; vertical lines denote the range of the transplanting and harvest dates of the proposed rice calendar; horizontal lines denote the range of the transplanting and harvest dates of the RiceAtlas rice calendar; dots denote the peak of the transplanting or harvest dates. Black dots denote the detected phenological day that falls within the transplanting or harvest ranges from the RiceAtlas rice calendar. Red and black solid lines represent the 1:1 line and regression, respectively.

3.2 Number of rice croppings

The number of rice croppings in the proposed rice calendar was obtained by counting the phenological dates for the three croppings (Fig. 10a). In comparison with the RiceAtlas (Fig. 10b), RICA (Fig. 10c), and SAGE (Fig. 10d) rice calendars based on the administrative scale, the proposed rice calendar shows the number of rice croppings per grid, which cannot be paralleled by the other rice calendars. Among the total of 4811 detected grids, 2728, 1644, and 439 grids were identified as single, double, and triple rice croppings, respectively. To compare the number of each rice cropping across the rice calendars with different spatial resolutions, the area for each number of croppings was calculated (Fig. 11). In the area calculation, the variation of the area of each grid cell on the ellipsoidal earth (Fig. S9) was considered, as was the percentage coverage of rice paddy fields in each grid (Fig. 1b).

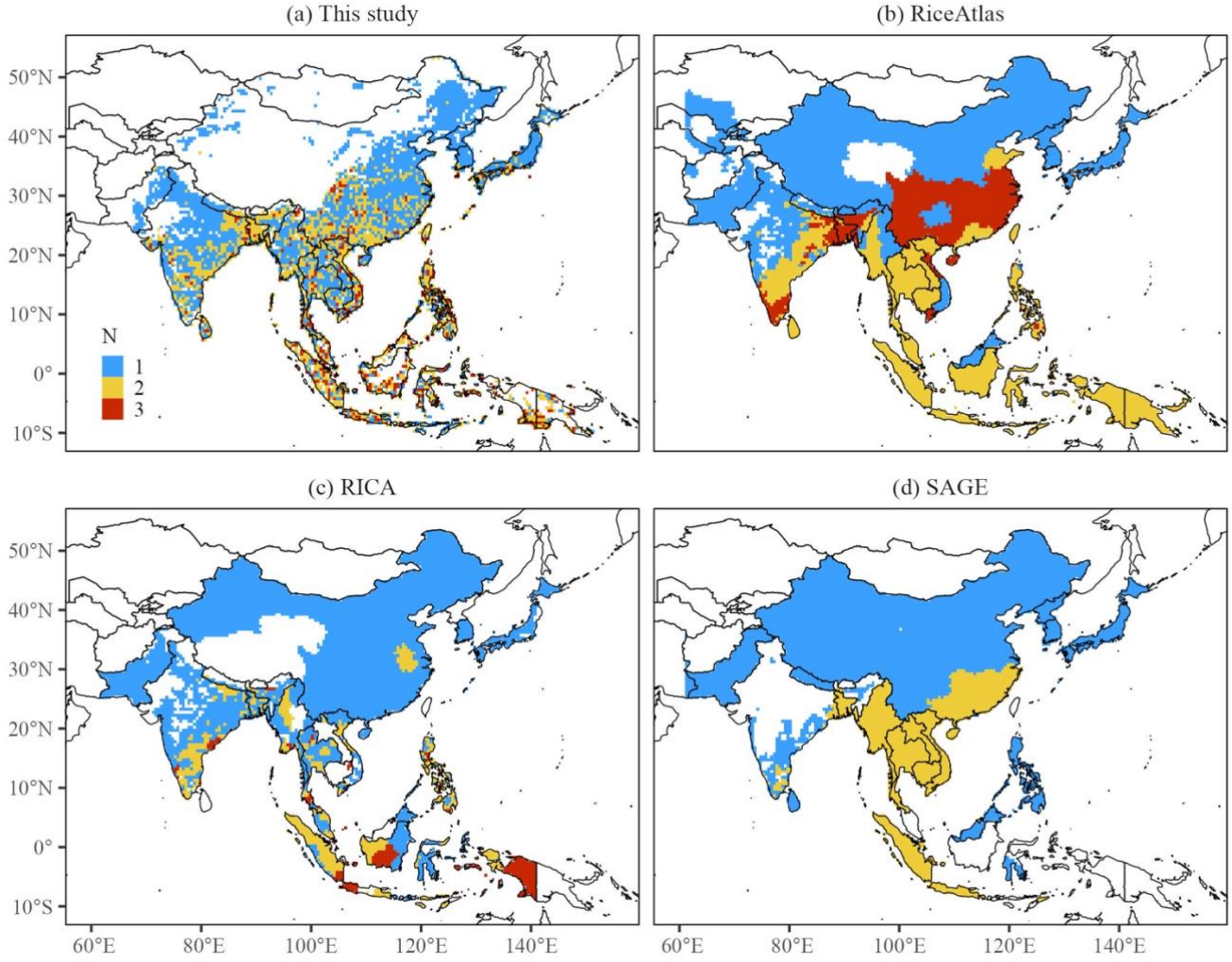

Figure 10. Detected number of rice croppings of **(a)** the proposed rice calendar, **(b)** the RiceAtlas rice calendar, **(c)** the RICA rice calendar, and **(d)** the SAGE rice calendar. Blue, yellow, and red colours represent single, double, and triple rice cropping, respectively.

355

The areas covered by single, double, and triple rice croppings in the proposed rice calendar are 0.53, 0.45, and 0.09 million of km^2, respectively (Fig. 11). The area covered by single rice cropping falls within the range of 0.24 (RiceAtlas rice calendar) to 0.65 million of km^2 (RICA rice calendar) (Fig. 11). The single rice cropping detection of the proposed rice calendar shows reasonable performance, with consistent detection across the north of the middle–lower reaches of the Yangtze River, North 360 Korea, South Korea, and most of Japan when compared with the other three rice calendars (Fig. 10). The regions of Haryana, Himachal Pradesh, and Punjab in India, central, midwestern, and western Nepal, and Balochistan, the Federally Administered Tribal Areas, and the North-West Frontier Province in Pakistan were also identified as single rice cropping areas (Fig. 10). In fact, these regions were initially identified as having double rice cropping, but they are dominated by the rice–wheat cropping

system (Abrol, 1997; Dhanda et al., 2022; Ahmad and Iram, 2023). Therefore, in this study, wheat cropping was removed within this region (Figs. 4–7, 10, 11, S10a, and S10b) (Abrol, 1997; Dhanda et al., 2022).

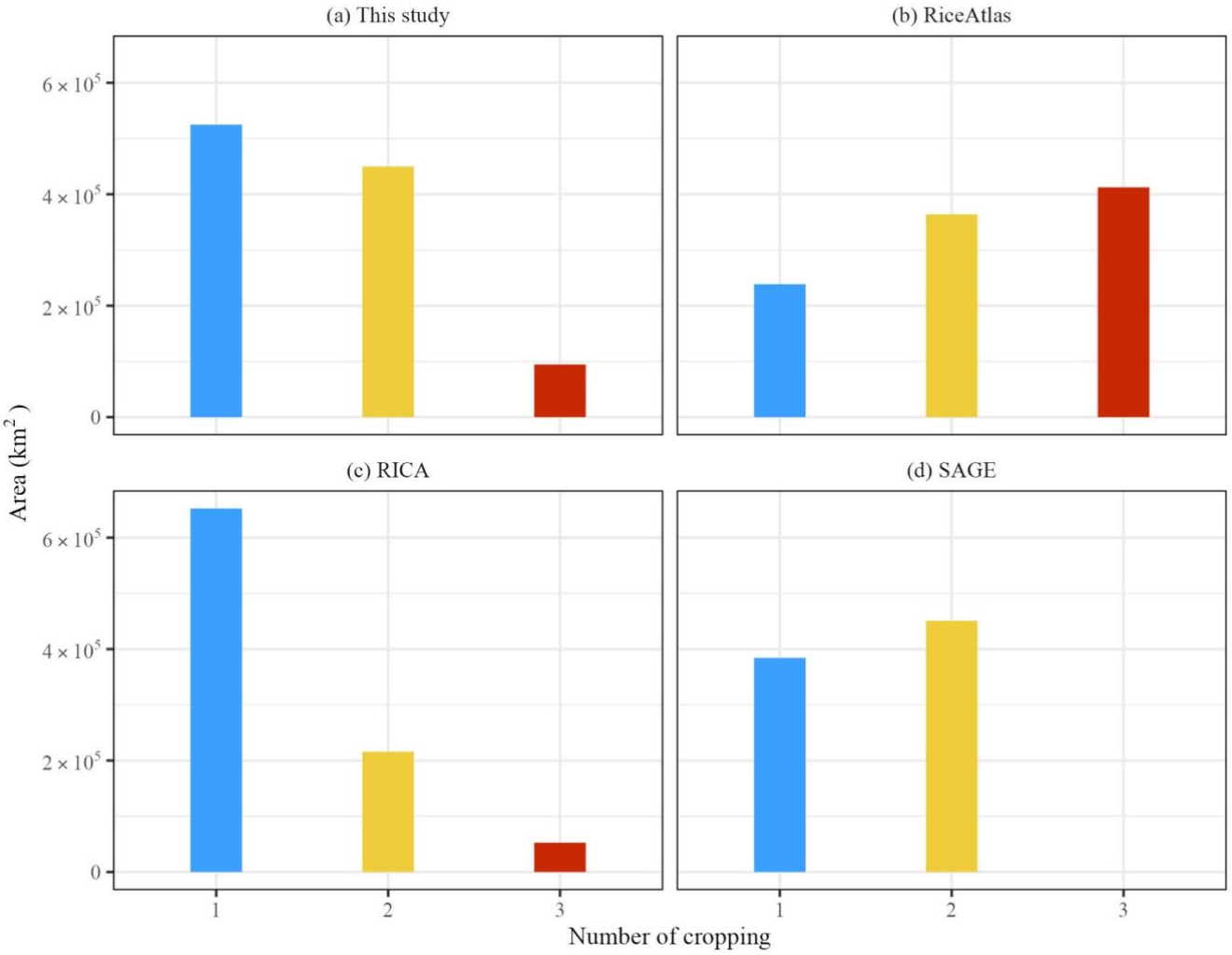

Figure 11. Area of rice cropping of **(a)** the proposed rice calendar, **(b)** the RiceAtlas rice calendar, **(c)** the RICA rice calendar, and **(d)** the SAGE rice calendar. Blue, yellow, and red colours represent single, double, and triple rice cropping, respectively.

The region of detected double rice cropping occupies a larger area in the proposed rice calendar than in the other three rice calendars (Fig. 11a). Additionally, the area covered by triple rice cropping falls within the range of 0.05 million of km^2 (RICA rice calendar) to 0.4 million of km^2 (RiceAtlas rice calendar). The proposed rice calendar successfully detects the mix of double and triple rice croppings in Southeast Asia, including Vietnam, Malaysia, Indonesia, and the Philippines. The results align with real-world observations. Double or triple rice croppings are mostly cultivated in Vietnam (Nguyen et al., 2012; Diem et al., 2021). Two main croppings are cultivated in Malaysia (Fatchurrachman et al., 2022) and the Philippines (Laborte et al.,

2012). Even on Java Island (Indonesia), the cultivation ranges from single to triple rice cropping systems (Ramadhani et al., 2020). In contrast, fewer areas of double rice cropping were detected in Myanmar, Thailand, Laos, and Cambodia using remote sensing-based methods such as the proposed calendar (Fig. 10a) and the RICA rice calendar (Fig. 10c), in comparison with census-based rice calendars such as the RiceAtlas (Fig. 10b) and SAGE (Fig. 10d) rice calendars. The presence of a large amount of small but highly heterogeneous rice paddy fields limits accurate detection of the number of rice croppings using remote sensing (Mishra et al., 2021). Moreover, census-based rice calendars record the potential number of rice cropping, which means that some rice croppings might overlap or that triple rice cropping is determined even though it accounts for only a small proportion of the rice cultivation activity within an administrative unit. This is a condition that does not occur in association with remote sensing-based rice calendars.

The proposed rice calendar extracts 9% of triple rice croppings (Fig. 11a), which are scattered and distributed in South China, Southeast Asia, and India (Fig. 10a). This proportion is close to that of the RICA rice calendar (6% in Fig. 11c), but markedly lower than that of the RiceAtlas rice calendar (41% in Fig. 11c). However, the larger percentage of triple rice croppings in the RiceAtlas rice calendar might be overestimated, especially in Northeast India and Bangladesh in areas of the lower Gangetic Plain. The double rice cropping system is predominant on the lower Gangetic Plain (Wang et al., 2020). In this area, rice cultivation occurs in one to three seasons, namely *Aus* (Mar/April/May to June/July), *Aman* (June/July/August to November/December), and *Boro* (November/December to January–April/May). Among the three seasons, *Aus* and *Aman* are the dominant croppings (Gunna et al., 2014; Singha et al., 2019). Similarly, in South China, which is dominated by double rice cropping, early rice is transplanted at the end of April and harvested at the end of July, while late rice is cultivated from June to October (Chen et al., 2020).

3.3 Advantages of the proposed rice calendar

The proposed rice calendar successfully extracts rice transplanting and harvest dates at 0.5° grid-cell scale across monsoon Asia by utilizing the rice feature-based phenology algorithm (Zhao et al., 2023) on Sentinel-1 and Sentinel-2 images (Fig. 2 Step 1 Algorithm a). The detected transplanting and harvest dates have been validated against 40 site-scale records from the literatures, showing high agreement with R^2 of 0.90 and 0.87, Bias of 7.99 and −9.07 days, MAE of 16.32 and 19.58 days, and RMSE of 19.00 and 22.43 days for transplanting and harvest dates, respectively (Supplementary Text 3.1). The robustness of the site validation (Fig. S12), combined with reasonable performance compared to other rice calendars (Fig. 9), further demonstrates the efficacy of the transplanting and harvest dates in the proposed rice calendar.

The main difference between the proposed rice calendar and other rice calendars lies in the algorithm for phenological date extraction. In contrast to census-based methods (such as the RiceAtlas rice calendar) that face the issue of overlapping rice croppings, and remote sensing-based methods (such as the RICA rice calendar) that rely on constant threshold values set for large areas, this algorithm is not limited by rice variety, management, and environmental factors. It extracts the features of

flooding around the transplanting date and peak yellowness during harvest from the minimum VH and peak NDYI values, respectively, without setting threshold parameters to characterize rice phenological variations. Unfortunately, due to the absence of ground-truth data, it is not possible to validate the Asian continental scale rice calendar with correct accuracy. Instead, the validation in this study was based on observational records available in the previous literature. In this validation, it is worth noting that the proposed rice calendar showed a relatively high coefficient of determination and low RMSE compared to other rice calendars (Supplementary Text 3.2).

~~The rice feature based phenology algorithm (Zhao et al., 2023) applied to Sentinel 1 and Sentinel 2 images (Fig. 2 Step 1 Algorithm a) successfully extracts rice transplanting and harvest dates at 0.5 grid cell scale across monsoon Asia. The robustness of validation at multiple spatial scales (Zhao et al., 2023), combined with reasonable performance in comparison with that of other rice calendars (Fig. 9), make the efficacy of the proposed rice calendar even more convincing. Furthermore, the proposed rice calendar outperforms the other rice calendars in terms of its algorithm for phenological date extraction. It overcomes the problem of overlap between rice croppings associated with census based methods (such as RiceAtlas rice calendar), and does not rely on algorithm with constant threshold values set for large areas, as is the case with other remote sensing based methods (such as RICA rice calendar). In contrast, this algorithm is not limited by rice variety, management, and environmental factors. Instead, the features of flooding around the transplanting date and the most yellowness when harvested are extracted from the minimum VH and peak NDYI values, respectively, without threshold parameter setting for characterizing rice phenological variations.~~

Detection of the number of rice croppings is another important part of the methodological framework of the proposed rice calendar. The fitted Weibull function, implemented in the R package (Fig. 2 Step 1 Algorithm b), automatically detects the number of rice croppings based on the shape of the smoothed EVI time series, facilitating rapid and efficient rice calendar mapping. The shape-based detection avoids identification of the number of rice croppings based on peak detection or on the occurrence of some certain phenological date within the rice season (e.g., flowering date, as in Mishra et al. (2021)). Additionally, the EVI shape-based detection allows identification of incomplete EVI arcs caused by non-continuous observations as one of the rice croppings (Fig. S2b).

Temporal and spatial integration of detected transplanting and harvest dates, as derived from Step 1, pose a great challenge owing to flexible agricultural schedules and the availability of satellite imagery. This limitation restricts widespread application of remote sensing-based rice calendars. In this study, a new algorithm (Fig. 2 Step 2) was proposed to address this problem, which has long been a challenge in the preparation of previous rice calendars (Mishra et al., 2021). The use of von Mises maximum likelihood estimates produces the average of the transplanting and harvest dates for 18 grids (3 × 3 grids × 2 years), taking the circular nature of phenological dates into special consideration (Fig. 2 Step 2d). This algorithm is of great benefit for application in tropical areas where rice growth continues throughout the year, let alone temperate areas where rice growth occurs once a year. Additionally, the superiority of this algorithm lies in its ability to consider all rice croppings instead of

excluding one of the rice cropping seasons through direct averaging based on administrative units. Furthermore, this algorithm improves the accuracy of the rice calendar by employing spatio-temporal integration, which reduces the presence of abnormal phenological dates.

The advantages of the above-mentioned algorithms (Fig. 2 Step 1, Step 2) largely contribute to the production of a gridded rice calendar. The proposed rice calendar provides spatially explicit rice phenology with continental coverage through remote sensing methods. The major difference between the proposed rice calendar and the RICA rice calendar lies in the use of a feature-based algorithm with VH and NDYI, which allows the proposed rice calendar to theoretically estimate rice phenology more accurately. Zhao et al. (2023) demonstrated that VH can accurately capture the start of paddy water logging, and NDYI is a good indicator of rice maturity stage. The proposed rice calendar presents a highly patchy map of rice phenological information (Figs. 6 and 10a). The 0.5° resolution of the proposed rice calendar is finer than that of other rice calendars, including the RiceAtlas, RICA at sub-national scale, and SAGE derived from sub-national data. This improvement greatly reduces the bias error caused by assigning averaged rice phenology to administrative units, as rice phenology can vary considerably within large administrative units (Franch et al., 2022). Furthermore, the proposed rice calendar displays the detailed distribution of rice paddy fields (Figs. 6 and 10a), in contrast to previous rice calendars that covered entire administrative areas, irrespective of the small proportion of rice cultivation (Figs. S6–S8 and 10b–d). Site-scale validation reinforces the above-mentioned advantages, as the phenological dates in the proposed rice calendar are closer to the in-site records (Fig. S13; Fig. S14; Supplementary Text 3). The relatively large bias and variance in other three rice calendars (Fig. S14) demonstrate their limitations and uncertainties in calculating the rice paddy field area as shown in Fig. 11.

3.4 Uncertainty

Although the potential and advantages of the proposed gridded rice calendar for monsoon Asia have been highlighted, some uncertainties remain. One challenge is the limited experimental periods on which the calendar is based, specifically during 2019–2020. While it was facilitated by the GEE and Google Colaboratory, generating detailed detection for two years (127 × 184 = 23,368 grids × 2 years) still requires large computation power. Additionally, errors can arise from the spatial and temporal integration of transplanting and harvest dates. The grouping process, in particular, poses a risk of assigning single rice cropping seasons from two years into different groups, potentially overestimating the number of rice croppings. Var parameter, derived from the mle.vonmises function (Eqs. (9) and (11)), is prone to bias, requiring bias-corrected estimates when the sample size is less than 16 (Best and Fisher, 1981). To address these issues, a 3 × 3 pixel window was used over two years to produce 18 values, highlighting the need to balance window size and sample size in spatio-temporal integration. The accuracy of reference rice calendars should also be considered, as they may rely on data from various sources and administrative scales (Laborte et al., 2017). Overlapping phenological dates between rice cropping seasons (Figs. S6–S8) can introduce further uncertainty. Furthermore, the complexity of multiple crop cropping systems can lead to an overestimation of the number of rice croppings. ~~rice croppings numbers.~~ The growth of ~~the~~ other crop exhibits a similar pattern of a mono-peaked

EVI time series and flood irrigation before sowing, similar to rice (Ahmad and Iram, 2023). Examples include the middle rice cropping system (rice with wheat, barley, or rapeseed cropping systems) in East and Central China (Chen et al., 2020) and the rice–wheat cropping systems on the Indo-Gangetic Plain (Abrol, 1997; Dhanda et al., 2022). Thus, detected triple rice in central China (Fig. 10a) will be bias, which requires specific noted when using it. Except for the rice-predominant areas, the rice–crop mixing problem can also puzzle the grids with a low rice percentage. While rice phenology extraction was obtained through randomly selected sampling of rice paddy fields from the 500 m resolution rice distribution map (Zhang et al., 2020), grids with a low rice percentage have a higher possibility of errors in wrongly classifying non-rice crops as rice, consequently resulting in the high possibility of non-rice crops being considered as rice cultivation or one of the rice croppings. The application of a higher resolution rice distribution map is expected to address this issue.

These uncertainties do not obscure the fact that this is a novel gridded rice calendar that provides more detailed rice phenology information, and could be input into ecosystem models for GHG emission evaluation and production prediction. With the continued efforts of the research community to increase the spatio-temporal resolution of earth observational data, integrated use of the new rice paddy field distribution map, and implementation of new tools for improved analysis of huge satellite images, it should become feasible to produce more precise rice calendars at finer scale. Meanwhile, the methodological framework developed in this study for mapping the proposed rice calendar provides robust reference for mapping other crop calendars.

4 Data availability

The developed Monsoon Asia Rice Calendar (MARC) ~~rice calendar~~ described in the manuscript is available at the Global Environmental Database (GED) https://www.nies.go.jp/doi/10.17595/20230728.001-e.html (Zhao and Nishina, 2023).

5 Code availability

The code for getting VH/EVI/NDYI time series data from Sentinel-1 and Sentinel-2 images, extracting the transplanting and harvest dates from smoothed VH/EVI/NDYI time series data, and spatial and temporal integration of detected transplanting and harvest dates can be found at https://db-test.cger.nies.go.jp/DL/10.17595/20230728.001.html.en (Zhao and Nishina, 2023).

6 Conclusions

Given the absence of an updated global/continental-scale rice calendar that can explicitly depict spatial gridded transplanting date and harvest date information, and the number of rice croppings, this study developed a new gridded rice calendar for

monsoon Asia with spatially explicit fine detail of rice phenology using a new methodological framework based on Sentinel-1 and Sentinel-2 images. Combination of a feature-based algorithm and a fitted Weibull function facilitates extraction of the transplanting and harvest dates and detection of number of rice croppings, respectively. Subsequently, the detected transplanting and harvest dates were subjected to temporal and spatial integration to produce the rice calendar. The proposed rice calendar was found sufficiently robust to map rice phenology more finely than that presented in other commonly used rice calendars, showing small Bias, ~~and improvement in both~~ MAE, and RMSE in terms of detection of transplanting and harvest dates. The proposed rice calendar could be used for global research on climate change and crop security, and the methodological framework could serve as a basis for producing large-scale mapping calendars for other crops.

Author contributions

KN conceived the conceptualization, acquired the funding, and supervised the project. XZ and KN developed the algorithm and curated the data. XZ, KN, and HI analysed the data. HI, SO, and SY contributed with satellite data analysis, and algorithm implementation. XZ and KN wrote the original draft, and XZ, KN, HI, YM, SO, and SY all reviewed the that draft.

Competing interests

The authors declare that they have no conflict of interest.

Financial support

This study was supported by the New Energy and Industrial Technology Development Organization (NEDO) (grant no. JPNP18016). This study was also partly supported by the Environment Research and Technology Development Fund (JPMEERF20202005) of the Environmental Restoration and Conservation Agency (ERCA).

References

Abrol, I.P.: Sustaining rice-wheat cropping system productivity in the Indo-Gangetic Plains, In: The 4th JIRCAS International Symposium, Sustainable Agricultural Development Compatible with Environmental Conservation in Asia, 26 August 1997, 155–1651, 1997.

Agostinelli, C. and Lund, U.: R package "circular": Circular Statistics (version 0.50). https://CRAN.R-project.org/package=circular, 2023.

Ahmad, I. and Iram, S.: Rice-wheat cropping pattern and resource conservation technologies: http://www.pakissan.com/english/agri.overview/rice.wheat.cropping.pattern.shtml, last access: 6 June 2023.

Berens, P.: CircStat: A MATLAB Toolbox for circular statistics, J. Stat. Softw., 31(10), 1–21, https://doi.org/10.18637/jss.v031.i10, 2019.

Best, D. and Fisher, N.: The BIAS of the maximum likelihood estimators of the von mises-fisher concentration parameters. Commun. Stat.-Simul. Comput., 10:5, 493–502, https://doi.org/10.1080/03610918108812225, 2007.

Boschetti, M., Busetto, L., Manfron, G., Laborte, A., Asilo, S., Pazhanivelan, S., and Nelson, A., PhenoRice: A method for automatic extraction of spatio-temporal information on rice crops using satellite data time series, Remote Sens. Environ., 194, 348–365, https://doi.org/10.1016/j.rse.2017.03.029, 2017.

Chen, C., Groenigen, K., Yang, H., Hungate, B., Yang, B., Tian, Y., Chen, J., Dong, W., Huang, S., Deng, A., Jiang, Y., and Zhang, W.: Global warming and shifts in cropping systems together reduce China's rice production, Glob. Food Secur., 24, 100359, https://doi.org/10.1016/j.gfs.2020.100359, 2020.

Clauss. K., Ottinger, M., Leinenkugel, P., and Kuenzer, C.: Estimating rice production in the Mekong Delta, Vietnam, utilizing time series of Sentinel-1 SAR data, Int. J. Appl. Earth Obs. Geoinf., 73, 574–585, https://doi.org/10.1016/j.jag.2018.07.022, 2018.

Dhanda, S., Yadav, A., Yadav, D.B., and Chauhan, B.S.: Emerging issues and potential opportunities in the rice-wheat cropping system of North-Western India, Front. Plant Sci. 13, 832683, https://doi.org/10.3389/fpls.2022.832683, 2022.

Diem, P.K., Diem, N.K., and Hung, H.V.: Assessment of the efficiency of using MODIS MCD43A4 in mapping of rice transplanting calendar in the Mekong Delta, IOP Conf. Ser.: Earth Environ Sci., 652, 012015, https://doi.org/10.1088/1755-1315/652/1/012015, 2021.

Elliott, J., Müller, C., Deryng, D., Chryssanthacopoulos, J., Boote, J., Büchner, M., Foster, I., Glotter, M., Heinke, J., Iizumi, T., Izaurralde, R.C., Mueller, N.D., Ray, D.K., Rosenzweig, C., Ruane, A.C., and Sheffield, J.: The global gridded crop model intercomparison: data and modeling protocols for phase 1 (v1.0), Geosci. Model Dev., 8, 261–277, https://doi.org/10.5194/gmd-8-261-2015, 2015.

FAOSTAT, (https://www.fao.org/faostat/en/#data), last access: 2 May 2023.

Fatchurrachman, Rudiyanto, Soh, N.C., Shah, R.M., Giap, S.G.E., Setiawan, B.I., and Minasny, B.: High-resolution mapping of paddy rice extent and growth stages across Peninsular Malaysia using a fusion of Sentinel-1 and 2 time series data in Google Earth Engine, Remote Sens., 14(8), 1875, https://doi.org/10.3390/rs14081875, 2022.

Franch, B., Cintas, J., Becker-Reshef, I., Sanchez-Torres, M.J., Roger, J., Skakun, S., Sobrino, J.A., Van Trichet, K., Degerickx, J., Gilliams, S., Koetz, B., Szantoi, Z., and Whitcraft, A.: Global crop calendars of maize and wheat in the framework of the WorldCreal project, GISci. Remote Sens., 59, 885–913, https://doi.org/10.1080/15481603.2022.2079273, 2022.

Iizumi, T., Kim, W., and Nishimori, M.: Modeling the global sowing and harvesting windows of major crops around the year 2000, J. Adv. Model. Earth Syst., 11(1), 99–112, https://doi.org/10.1029/2018MS001477, 2019.

Inoue, S., Ito, A., and Yonezawa, C.: Mapping paddy fields in Japan by using a Sentinel-1 SAR time series supplemented by Sentinel-2 images on Google Earth Engine, Remote Sens., 12(10), 1622, https://doi.org/10.3390/rs12101622, 2020.

Ito, A., Inoue, S., and Inatomi, M.: Model-based evaluation of methane emissions from paddy fields in East Asia, J. Agric. Meteorol., 78(2), 56–65, https://doi.org/10.2480/agrmet.D-21-00037, 2022.

Jiang, Y., Carrijo, D., Huang, S., Chen, J., Balaine, N., Zhang, W., van Groenigen K.J., and Linquist, B.: Water management to mitigate the global warming potential of rice systems: A global meta-analysis, Field Crop Res., 234, 47–54, https://doi.org/10.1016/j.fcr.2019.02.010, 2019.

Kotsuki, S. and Tanaka, K.: SACRA-A method for the estimation of global high-resolution crop calendars from satellite-sensed NDVI, Hydrol. Earth Syst. Sci., 19(11), 4441–4461, https://doi.org/10.5194/hess-19-4441-2015, 2015.

Laborte, A.G., Bie, K.D., Smaling, E.M.A., Moya, P.F., Boling, A.A., and Ittersum, M.K.V.: Rice yields and yield gaps in southeast Asia: past trends and future outlook. Eur. J. Agron., 36(1), 9–20, https://doi.org/10.1016/j.eja.2011.08.005, 2012.

Laborte, A.G., Gutierrez, M.A., Balanza, J.G., Saito, K., Zwart, S.J., Boschetti, M., Murty, M.V.R., Villano, L., Aunario, J.K., Reinke, R., Koo, J., Hijmans, R.J., and Nelson, A.: RiceAtlas, a spatial database of global rice calendars and production, Sci. Data, 4, 170074, https://doi.org/10.1038/sdata.2017.74, 2017.

Liu, S., Chen, Y., Ma, Y., Kong, X., Zhang, X., and Zhang, D.: Mapping ratoon rice transplanting area in Central China using Sentinel-2 time stacks and the phenology-based algorithm, Remote Sens., 12(20), 3400, https://doi.org/10.3390/rs12203400, 2020.

Luo, Y., Zhang, Z., Chen, Y., Li, Z., and Tao, F.: ChinaCropPhen1km: a high-resolution crop phenological dataset for three staple crops in China during 2000-2015 based on leaf area index (LAI) products, Earth Syst. Sci. Data, 12, 197–214, https://doi.org/10.5194/essd-12-197-2020, 2020.

Maciel-Nájera, J.F., Hernández-Velasco, J., Gonzalez-Elizondo M.S., Hernandez-Díaz, J.C., López-Sánchez C.A., Antúnez, P., Bailón-Soto C.E., and Wehenkel, C.: Unexpected spatial patterns of natural regeneration in typical uneven-aged mixed pine-oak forests in the Sierra Madre Occidental, Mexico, Glob. Ecol. Conserv., 23, e01074, https://doi.org/10.1016/j.gecco.2020.e01074, 2020.

Mahan, R.: Circular statistical methods: applications in spatial and temporal performance analysis, U.S. Army Research Inst. for Behavioral and Social Sciences, Final Rep. 1991.

Mathison, C., Deva, C., Falloon, P., and Challinor, A.J.: Estimating sowing and harvest dates based on the Asian summer monsoon, Earth Syst. Dynam., I, 563–592, https://doi.org/10.5194/esd-9-563-2018, 2017.

Mishra. B., Busetto, L., Boschetti, M., Laborte, A., and Nelson, A.: RICA: A rice crop calendar for Asia based on MODIS multi year data, Int. J. Appl. Earth Obs. Geoinf., 103, 102471, https://doi.org/10.1016/j.jag.2021.102471, 2021.

More, R.S., Manjunath, K.R.,Jain, N.K., Panigraphy, S., and Parihar, J.S.: Derivation of rice crop calendar and evaluation of crop phenometrics and latitudinal relationship for major south and south-east Asian countries: A remote sensing approach. Comput. Electron. Agric., 127, 336–350, https://doi.org/10.1016/j.compag.2016.06.026, 2016.

Muñoz-Salazar, T., LeQuesne, C., Rozas, V., Christie, D.A., and Rojas-Badilla, M.: Examining the potential of Austrocedrus chilensis tree rings as indicators of past late-spring forest events in central Chile, Dendrochronologia, 74, 125962, https://doi.org/10.1016/j.dendro.2022.125962, 2022.

Nguyen, T.T.H., De Bie, C.A.J.M., Ali, A., Smaling, E.M.A., and Chu, T. H.: Mapping the irrigated rice cropping patterns of the Mekong delta, Vietnam, through hyper-temporal SPOT NDVI image analysis, Int. J. Remote Sens., 33(2), 415–434, https://doi.org/10.1080/01431161.2010.532826, 2012.

Pandey, S., Mortimer, M., Wade, L., Tuong, TP., Lopez, K., and Hardy, B. (Eds): Direct seeding: research issues and opportunities, in: Proceedings of the International Workshop on Direct Seeding in Asia Rice Systems: Strategic Research Issues and Opportunities, Bangkok, Thailand, 25–28 January, 2000.

Portmann, F.T., Siebert, S., and Döll, P.: MIRCA2000-Global monthly irrigated and rainfed crop areas around year 2000: A new high-resolution data set for agricultural and hydrological modelling, Glob. Biogeochem. Cycle, 24, GB1011, https://doi.org/10.1029/2008GB003435, 2010.

Ramadhani, F., Pullanagari, R., Kereszturi, G., and Procter, J.: Automatic mapping of rice growth stages using the integration of Sentinel-2, MOD13Q1, and Sentinel-1, Remote Sens., 12(21), 3613, https://doi.org/10.3390/rs12213613, 2020.

Rolinski, S., Horn, H., Petzoldt, T., and Paul, L.: Identifying cardinal dates in phytoplankton time series to enable the analysis of long-term trends, Oecologia, 153(4), 997–1008, https://doi.org/10.1007/s00442-007-0783-2, 2007.

Sacks, W.J., Deryng, D., Foley, J.A., and Ramankutty, N.: Crop transplanting dates: An analysis of global patterns, Glob. Ecol. Biogeogr., 19, 607–620, https://doi.org/10.1111/j.1466-8238.2010.00551.x, 2010.

Sakamoto, T., Yokozawa, M., Toritani, H., Shibayama, M., Ishitsuka, N., and Ohno, H.: A crop phenology detection method using time-series MODIS data, Remote Sens. Environ., 96, 366–374, https://doi.org/10.1016/j.rse.2005.03.008, 2005.

Saunois, M., Stavert, A.R., Poulter, B., Bousquet, P., Canadell, J.G., Jackson, R.B., Raymond, P.A., Dlugokencky, E.J., Houweling, S., Patra, P.K., Ciais, P., Arora, V.K., Bastviken, D., Bergamaschi, P., Blake, D.R., Brailsford, G., Bruhwiler, L., Carlson, K.M., Carrol, M., Castaldi, S., Chandra, N., Crevoisier, C., Crill, P.M., Covey, K., Curry, C.L., Etiope, G., Frankenberg, C., Gedney, N., Hegglin, M.I., Höglund-Isaksson, L., Hugelius, G., Ishizawa, M., Ito, A., Janssens-Maenhout, G., Jensen, K.M., Joos, F., Kleinen, T., Krummel, P.B., Langenfelds, R.L., Laruelle, G.G., Liu, L., Machida, T., Maksyutov, S., McDonald, K.C., McNorton, J., Miller, P.A., Melton, J.R., Morino, I., Müller, J., Murguia-Flores, F., Naik, V., Niwa, Y., Noce, S., O'Doherty, S., Parker, R.J., Peng, C., Peng, S., Peters, G.P., Prigent, C., Prinn, R., Ramonet, M., Regnier, P., Riley, W.J., Rosentreter, J.A., Segers, A., Simpson, I.J., Shi, H., Smith, S.J., Steele, L.P., Thornton, B.F., Tian, H., Tohjima, Y., Tubiello, F.N., Tsuruta, A., Viovy, N., Voulgarakis, A., Weber, T.S., van Weele, M., van der Werf, G.R., Weiss, R.F.,Worthy, D., Wunch, D., Yin, Y., Yoshida, Y., Zhang, W., Zhang, Z., Zhao, Y., Zheng, B., Zhu, Q., Zhu, Q., and Zhuang, Q.: The global methane budget 2000–2017, Earth Syst. Sci. Data, 12, 1561–1623, https://doi.org/10.5194/essd-12-1561-2020, 2020.

Singha. M., Dong, J., Zhang, G., and Xiao, X.: High resolution paddy rice maps in cloud-prone Bangladesh and Northeast India using Sentinel-1 data, Sci. Data, 6, 1–10, https://doi.org/10.1038/s41597-019-0036-3, 2019.

Torres, R., Snoeij, P., Geudtner, D., Bibby, D., Davidson, M., Attema, E., Potin, P., Rommen, B., Floury, N., Brown, M., Traver, I.N., Deghaye, P., Duesmann, B., Rosich, B., Miranda, N., Bruno, C., L'Abbate, M., Croci, R., Pietropaolo, A., Huchler, M., and Rostan, F.: GMES Sentinel-1 mission, Remote Sens. Environ., 120, 9–24, https://doi.org/10.1016/j.rse.2011.05.028, 2012.

Waha., K., van Bussel, G.J., Müller, C., and Bondeau, A.: Climate-drive simulation of global crop sowing dates, Glob. Ecol. Biogeogr., 21, 247–259, https://doi.org/10.1111/j.1466-8238.2011.00678.x, 2012.

Wang, X., Wang, S., Li, X., Chen, B., Wang, J., Huang, M., and Rahman, A.: Modelling rice yield with temperature optima of rice productivity derived from satellite NIRv in tropical monsoon area, Agric. For. Meteorol., 294, 108135, https://doi.org/10.1016/j.agrformet.2020.108135, 2020.

Xiao, W., Xu, S., He, and T.: Mapping paddy rice with Sentinel-1/2 phenology-, object-based algorithm-a implementation in Hangjiahu in China using GEE platform, Remote Sens., 13(5), 990, https://doi.org/10.3390/rs13050990, 2021.

Xin, Q., Li, J., Li, Z., Li, Y., and Zhou, X.: Evaluations and comparisons of rule-based and machine-learning-based methods to retrieve satellite-based vegetation phenology using MODIS and USA National Phenology Network data, Int. J. Appl. Earth Obs. Geoinf., 93, 102189, https://doi.org/10.1016/j.jag.2020.102189, 2020.

Yan, H., Liu, F., Qin, Y., Doughty, R., and Xiao, X.: Tracking the spatio-temporal change of cropping intensity in China during 2000-2015, Environ. Res. Lett., 14, 035008, https://doi.org/10.1088/1748-9326/aaf9c7, 2019.

Yang, Q., Shi, L., Han, J., Yu, J., and Huang, K.: A near real-time deep learning approach for detecting rice phenology based on UAV images. Agric. For. Meteorol., 287, 107938, https://doi.org/10.1016/j.agrformet.2020.107938, 2020.

Zhang, G., Xiao, X., Dong, J., Xin, F., Zhang, Y., Qin, Y., Doughty, R.B., and Moore, B.: Fingerprint of rice paddies in spatial–temporal dynamics of atmospheric methane concentration in monsoon Asia, Nat. Commun., 11, 554, https://doi.org/10.1038/s41467-019-14155-5, 2020.

Zhang, J., Wu, H., Zhang, Z., Zhang, L., Luo, Y., Han, J., and Tao, F.: Asian rice calendar dynamics detected by remote sensing and their climate drivers, Remote Sens., 14(17), 4189, https://doi.org/10.3390/rs14174189, 2022.

Zhang, M., Wu, B., Zeng, H., He, G., Liu, G., Tao, S., Zhang, Q., Nabil, M., Tian, F., Bofana, J., Bayene, A.N., Elnashar, A., Yan, N., Wang, Z., and Liu, Y.: GCI30: a global dataset of 30 m cropping intensity using multisource remote sensing imagery, Earth Syst. Sci. Data, 13, 4799–4817, https://doi.org/10.5194/essd-13-4799-2021, 2021a.

Zhang, W., Peng, K., Cui, F., Wang, D., Zhao, J., Zhang, J., Yu, N., Wang, Y., Zeng, D., Wang, Y., Cheng, Z., and Zhang, K.: Cytokinin oxidase/dehydrogenase OsCKX11 coordinates source and sink relationship in rice by simultaneous regulation of leaf senescence and grain number, Plant Biotechnol., J. 19(2), 335–350, https://doi.org/10.1111/pbi.13467, 2021b.

Zhao, X., Nishina, K., Akitsu, T.K., Jiang, L., Masutomi, Y., and Nasahara, K.N.: Feature-based algorithm for large-scale rice phenology detection based on satellite images, Agric. For. Meteorol., 329, 109283, https://doi.org/10.1016/j.agrformet.2022.109283, 2023.

Zhao, X. and Nishina, K.: Monsoon Asia Rice Calendar: a gridded rice calendar in monsoon Asia based on Sentinel-1 and Sentinel-2 images [data set], NIES, https://www.nies.go.jp/doi/10.17595/20230728.001-e.html, 2023.